Available online at www.sciencedirect.com
SCIENCE DIRECT
Journal of Sound and Vibration 295 (2006) 531–552
JOURNAL OF SOUND AND VIBRATION
www.elsevier.com/locate/jsvi

Input/output versus output-only data processing for structural identification—Application to in-flight data analysis

Laurent Mevel[a], Albert Benveniste[a], Michèle Basseville[a,c,*], Maurice Goursat[b], Bart Peeters[d], Herman Van der Auweraer[d], Antonio Vecchio[d]

[a]*IRISA, Campus de Beaulieu, 35042 Rennes Cedex, France*
[b]*INRIA, BP 105, Rocquencourt, 78153 Le Chesnay Cedex, France*
[c]*CNRS, France*
[d]*LMS International, Researchpark Haasrode Z1, Interleuvenlaan 68, 3001 Leuven, Belgium*

Received 23 November 2004; received in revised form 16 December 2005; accepted 3 January 2006
Available online 11 April 2006

Abstract

The problem of structural model identification under *both* known and unknown input excitations, is addressed. In-flight data analysis is an important instance of that problem. Input/output and output-only eigenstructure identification methods are described and compared, within two classes of methods: subspace-based and prediction error. In particular, different types of relevant projections for handling the known and unknown inputs are discussed. The relevance of the methods is emphasized through numerical results obtained on real flight test data sets.

1. Introduction

System identification and parameter estimation from flight data sets is a research *and* industrial topic of growing interest for flight vehicule design and certification [1]. For in-flight structural model identification, the handling of both known (measured) and unknown (often non-stationary) input excitations is mandatory [2]. This topic is the subject of the present paper. Before outlining its content, both practical and conceptual motivations are provided for the structural identification methods which are investigated here.

1.1. Practical motivations

Experimental modal analysis (EMA) is currently one of the key technologies in structural dynamics analysis. Based on the academic foundations of system identification, it has evolved to become a ''standard'' approach in mechanical product development. Essential in this evolution is that modal analysis research has, from the start, taken the point of view of industrial applicability, focusing on solving the specific problems related to testing and modeling large industrial structures (see also Section 4.4). The merit of each new method

*Corresponding author. Tel.: +33 2 99 84 72 36; fax: +33 2 99 84 71 71.
E-mail address: basseville@irisa.fr (M. Basseville).

0022-460X/$ - see front matter © 2006 Elsevier Ltd. All rights reserved.
doi:10.1016/j.jsv.2006.01.039

or new approach has always been checked against the added value it brought in terms of helping the application engineers to derive better models.

A nice example is the development cycle of a new aircraft, which consists of several modeling and testing stages: structural finite element (FE) modeling, ground vibration testing (GVT), computational fluid dynamics (CFD) modeling, wind tunnel testing, and in-flight tests. These flight (vibration) tests allow the validation of the analytical models under various real flight conditions and, more important, allow to assess, as a function of airspeed and altitude, the aero-elastic interaction between the structure and the aerodynamic forces as they may lead to a sudden unstable behavior known as flutter. Flutter shows up in the vibration signals as apparent negative damping and corresponding sudden increase of the vibration amplitudes. For economic and safety reasons, it is evidently avoided that an aircraft undergoes flutter during an in-flight test, but it has to be certified that it has sufficient flutter margin when flying at the different points of the flight envelope where it is designed for. To determine this margin, typically, the trends of eigenfrequencies and damping ratios of the critical modes as a function of airspeed are carefully studied [3,2]. This explains the need to perform system identification during the flight.

Current practice is to apply and measure artificial excitation (the inputs) during the flight and measure the aircraft acceleration response at various locations (the outputs). Various solutions were developed to provide this dynamic excitation during the flight such as excitation through the control surfaces or wing-tip excitation by aerodynamic vanes [3]. A recent trend in flight-testing is the use of atmospheric turbulences as additional excitation sources, from which it is expected that a better exploitation of flight test data, and a wider exploration of the flight domain, can be achieved. In this case, the typical situation is that it is practically impossible to measure those forces acting on the aircraft, and that the deterministic knowledge for those inputs is replaced by a white noise assumption.

1.2. Conceptual motivations

It is known [4–6] that the modes and mode-shapes of a mechanical structure coincide with the eigenstructure of a continuous time multiple input multiple output (MIMO) linear system driven by an excitation, and whose output vector is the set of accelerometer measurements. Because of what has been argued above, the key issue is to identify the eigenstructure in the presence of *both* a natural (unknown, unmeasured and often non-stationary) excitation and a known (measured) input. This set up is often referred to as *input/output* [7].

Handling both known and unknown excitations inputs should take advantage of the available knowledge on the inputs, and thus should rely on input/output identification methods. However, it is of interest to understand that involving the input data can be done with *minor* modification of output-only identification methods to be used for eigenstructure identification in-operation, that is in the presence of natural excitation [8,9].

During the last decade, there has been a growing interest in subspace-based linear system identification methods [10–12]. These time domain methods, which process either raw data or correlation matrices, are well suited for capturing the system eigenstructure, even without observed inputs [8]. On the other hand, the recent frequency domain polyreference least-squares complex frequency (LSCF) method [13–15] is a special implementation of a matrix fraction description-based prediction error method (PEM) for eigenstructure identification. It handles Fourier transformed data, and can be run under either input/output or output-only form, using frequency response functions (FRF) or power spectra, respectively.

The purpose of this paper is to discuss different types of projections which can be performed for handling, separately or simultaneously, the known and unknown inputs within the framework of the covariance driven subspace-based *time domain* structural identification method; to review the recent *frequency domain* polyreference LSCF input/output and output-only eigenstructure identification methods and re-cast them in a framework closely related to the subspace methods; and to investigate the relevance of both classes of methods for in-flight data analysis by reporting on numerical results obtained on real data sets.

1.3. Paper outline

In Section 2, the key elements of *subspace-based covariance-driven* eigenstructure identification are recalled, and how to process *time-domain* input/output data and to handle both known and unknown inputs, is

explained. In Section 3, the key elements of a recent *matrix fraction description*-based implementation of the PEM are introduced under both input/output and output-only forms, and related to the subspace-based methods. In Section 4, implementation issues and industrial testing requirements are addressed. In Section 5, numerical results obtained on real flight data sets are reported, and the two types of methods and input handling are discussed. Section 6 contains further comments and conclusions.

2. Subspace-based eigenstructure identification

The widespread use of state-space representations for modal analysis [4,5,8,16] relies on the fact that the eigenstructure of the state transition matrix $\mathbf{F}$ of a discrete time linear model:

$$\begin{cases} \mathbf{X}_k = \mathbf{F}\mathbf{X}_{k-1} + \mathbf{W}_k, \\ \mathbf{Y}_k = \mathbf{H}\mathbf{X}_k, \end{cases} \tag{1}$$

is in one-to-one correspondence with the structural modes (eigenvalues) and mode-shapes (eigenvectors); see Appendix. The use of either covariance- or data-driven subspace-based identification algorithms for structural analysis has thus been advocated [17,18,8,9]. Covariance-driven algorithms might be appealing when processing long samples of multi-sensor output measurements, which can be mandatory for in-operation modal analysis under non-stationary environment. In this section, we describe covariance-driven subspace-based identification algorithms for the combined handling of known and unknown inputs.

2.1. Fundamentals of covariance-driven identification algorithms

Throughout the paper, we use repeatedly the following elementary remark, which belongs to the folklore of system or matrix theory. Consider a pair $(\mathbf{H}, \mathbf{F})$ of matrices, respectively $r \times n$ and $n \times n$. Let $\mathbf{R} \triangleq (\mathbf{R}_i)_{i \geqslant 0}$ be a sequence of matrices such that $\mathbf{R}_i$ decomposes as

$$\mathbf{R}_i = \mathbf{H}\mathbf{F}^{i-1}\mathbf{G} \tag{2}$$

for some matrix $\mathbf{G}$, independent from i. Then the (infinite) Hankel matrix:

$$\mathscr{H}(\mathbf{R}) \triangleq \begin{bmatrix} \mathbf{R}_1 & \mathbf{R}_2 & \mathbf{R}_3 & \mathbf{R}_4 & \dots \\ \mathbf{R}_2 & \mathbf{R}_3 & \mathbf{R}_4 & \mathbf{R}_5 & \dots \\ \mathbf{R}_3 & \mathbf{R}_4 & \mathbf{R}_5 & \mathbf{R}_6 & \dots \\ \dots & \dots & \dots & \dots & \dots \end{bmatrix} \tag{3}$$

factors out as: $\mathscr{H}(\mathbf{R}) = \Gamma(\mathbf{H}, \mathbf{F})\Xi(\mathbf{F}, \mathbf{G})$, where: $\Gamma(\mathbf{H}, \mathbf{F}) \triangleq \begin{bmatrix} \mathbf{H} \\ \mathbf{H}\mathbf{F} \\ \mathbf{H}\mathbf{F}^2 \\ \vdots \end{bmatrix}$ and $\Xi(\mathbf{F}, \mathbf{G}) \triangleq [\mathbf{G} \ \ \mathbf{F}\mathbf{G} \ \ \mathbf{F}^2\mathbf{G} \ \ \dots]$. Such a factorization is unique up to a post-multiplication of $\Gamma(\mathbf{H}, \mathbf{F})$ by an invertible matrix. Then, up to a change of basis on $\mathbf{F}$, the pair $(\mathbf{H}, \mathbf{F})$ can be recovered, respectively, from the first block-row and the shift invariance property of $\Gamma(\mathbf{H}, \mathbf{F})$, namely:

$$\Gamma^{\uparrow}(\mathbf{H}, \mathbf{F}) = \Gamma(\mathbf{H}, \mathbf{F})\mathbf{F} \quad \text{where } \Gamma^{\uparrow}(\mathbf{H}, \mathbf{F}) \triangleq \begin{bmatrix} \mathbf{H}\mathbf{F} \\ \mathbf{H}\mathbf{F}^2 \\ \vdots \end{bmatrix}. \tag{4}$$

Two important instances of the factorization in Eq. (2) come out with state-space system in Eq. (1).

- The first case is when the sequence $(\mathbf{W}_k)$ is a white noise, and the matrices $\mathbf{R}_i$'s are the output covariance matrices: $\mathbf{R}_i \triangleq E(\mathbf{Y}_k \mathbf{Y}_{k-i}^{\mathrm{T}})$, where $E(.)$ denotes the expectation operator. In that case, $\mathbf{G}$ is the cross-covariance between the state and the output vectors: $\mathbf{G} \triangleq E(\mathbf{X}_k \mathbf{Y}_k^{\mathrm{T}})$.

- The second case is when the sequence $(\mathbf{W}_k)$ is a measured and white input, and the matrices $\mathbf{R}_i$'s are the input/output cross-covariance matrices: $\mathbf{R}_i \triangleq E(\mathbf{Y}_k \mathbf{W}_{k-i}^{\mathrm{T}})$. In that case, $\mathbf{G}$ is the state/input cross-covariance: $\mathbf{G} \triangleq E(\mathbf{X}_k \mathbf{W}_k^{\mathrm{T}})$.

In both cases, the technique sketched above applies, and the system eigenstructure is then extracted from $\mathbf{F}$. Subspace-based structural identification is known to be a key instance of that. See Section 4.1 for the implementation details.

All the algorithms introduced in this section are based on this approach. Fed with selected input and output data covariance matrices, they all handle factorizations in the form of Eq. (2), with an *identical* left factor $\mathbf{HF}^i$. Different measured and/or projected data covariances are used, possibly in a combined manner thanks to the unique left factor.

2.2. Handling time domain input/output data

We consider a linear time-invariant state space system with a *combined* known input excitation $\mathbf{U}_k$ and unknown ambient excitation $\mathbf{V}_k$:

$$\begin{cases} \mathbf{X}_k = \mathbf{F}\mathbf{X}_{k-1} + \mathbf{D}\mathbf{U}_k + \mathbf{V}_k, & \mathbf{cov}(\mathbf{V}_k) = \mathbf{Q}_V, \\ \mathbf{Y}_k = \mathbf{H}\mathbf{X}_{k-1} + \varepsilon_k, & \mathbf{cov}(\varepsilon_k) = \mathbf{Q}_\varepsilon, \end{cases} \tag{5}$$

where $(\mathbf{U}_k)$ is the known input, the unknown noises $(\mathbf{V}_k)$ and (ε_k) are zero mean Gaussian white noise sequences, and the three sequences $(\mathbf{U}_k), (\mathbf{V}_k)$ and (ε_k) are pairwise uncorrelated. Note that the measurement noise (ε_k) does not affect the eigenstructure of the system in Eq. (5), and that a moving average sequence (ε_k) can also be encompassed [12,16]. The different signals, and in particular the known input vector $(\mathbf{U}_k)$, are assumed to be stationary.[1] Furthermore, because of what is explained above, we assume that:

$$\text{Known } \mathbf{U}_k \text{ and unknown } \mathbf{V}_k \text{ inputs are uncorrelated,} \tag{6}$$

$$\text{Unknown input } \mathbf{V}_k \text{ is white,} \tag{7}$$

$$\text{White measurement noise } \varepsilon_k \text{ is uncorrelated from both } \mathbf{U}_k \text{ and } \mathbf{V}_k. \tag{8}$$

For recovering the eigenstructure of Eq. (5), our approach consists in handling different projections of the system onto the subspace generated by *all* the known inputs, or onto its orthogonal subspace. Formally, the set of zero mean finite covariance vector random variables is equipped with the scalar product: $\langle \mathbf{W}, \mathbf{Z} \rangle \triangleq E(\mathbf{WZ})$. Let $\mathscr{U}$ denote the linear space generated by all the known inputs: $\mathscr{U} = \mathrm{Span}\{\mathbf{U}_j : -\infty < j < +\infty\}$. Its orthogonal complement is denoted by $\mathscr{U}^\perp$. Recovering the eigenstructure of Eq. (5) can be performed by using the following approaches:[2]

A1. Eliminating the unknown input $\mathbf{V}$ by projecting Eq. (5) onto $\mathscr{U}$.
A2. Eliminating the known input $\mathbf{U}$ by projecting Eq. (5) onto $\mathscr{U}^\perp$.
A3. Using jointly both projections of Eq. (5) onto $\mathscr{U}$ and $\mathscr{U}^\perp$—Variant 1.
A4. Using jointly both projections of Eq. (5) onto $\mathscr{U}$ and $\mathscr{U}^\perp$—Variant 2.
A5. Ignoring the presence of the known input $\mathbf{U}$.

Using projections in combination with subspace algorithms is a very natural idea that is found in several places in Ref. [12]. However, as the experienced reader will recognize, we exploit this idea under non-classical variants. The following notation is used throughout. For $(\mathbf{W}_k)_{k\in Z}$ and $(\mathbf{Z}_k)_{k\in Z}$ two stationary zero mean

[1] Arguments similar to those in Refs. [19,20] can be used for relaxing this assumption; this will be addressed elsewhere.

[2] Since the system in Eq. (5) is *dynamical*, it is mandatory to project it on shift-invariant subspaces, this is why *all* the known input variables are considered in $\mathscr{U}$.

vector random processes, we set:

$$\mathbf{R}_i^{WZ} \triangleq E(\mathbf{W}_k \mathbf{Z}_{k-i}^{\mathrm{T}}). \tag{9}$$

The algorithms A1–A5 are now described. Except for Algorithm A2, they all require $(\mathbf{U}_k)$ to be white.

2.2.1. Algorithm A1: eliminating the unknown input

For this algorithm, $(\mathbf{U}_k)$ is assumed white. Thanks to assumptions in Eqs. (6) and (8), projecting Eq. (5) onto $\mathscr{U}$ amounts to eliminating the unknown input. This projection writes:

$$\begin{cases} \mathbf{X}_k/\mathscr{U} = \mathbf{F}\mathbf{X}_{k-1}/\mathscr{U} + \mathbf{D}\mathbf{U}_k, \\ \mathbf{Y}_k/\mathscr{U} = \mathbf{H}\mathbf{X}_{k-1}/\mathscr{U}. \end{cases} \tag{10}$$

Setting for short $\mathbf{Z}^{\mathscr{U}} \triangleq \mathbf{Z}/\mathscr{U}$ when there is no risk of confusion, Eq. (10) rewrites:

$$\begin{cases} \mathbf{X}_k^{\mathscr{U}} = \mathbf{F}\ \mathbf{X}_{k-1}^{\mathscr{U}} + \mathbf{D}\mathbf{U}_k, \\ \mathbf{Y}_k^{\mathscr{U}} = \mathbf{H}\ \mathbf{X}_{k-1}^{\mathscr{U}}. \end{cases} \tag{11}$$

Using the notation in Eq. (9), thanks to the assumption in Eq. (7), and *assuming additionally* $(\mathbf{U}_k)$ *white*, the relations in Eq. (11) give rise to decompositions of the form in Eq. (2) for the covariance matrices $\mathbf{R}_i^{Y^{\mathscr{U}}Y^{\mathscr{U}}}$ and $\mathbf{R}_i^{Y^{\mathscr{U}}U}$:

$$\mathbf{R}_i^{Y^{\mathscr{U}}Y^{\mathscr{U}}} = \mathbf{H}\mathbf{F}^{i-1}\mathbf{G}^{Y}, \quad \text{where } \mathbf{G}^{Y} \triangleq E(\mathbf{X}_k^{\mathscr{U}}\mathbf{Y}_k^{\mathscr{U}\mathrm{T}}) = \mathbf{R}_0^{X^{\mathscr{U}}Y^{\mathscr{U}}}, \tag{12}$$

$$\mathbf{R}_i^{Y^{\mathscr{U}}U} = \mathbf{H}\mathbf{F}^{i-1}\mathbf{G}^{U}, \quad \text{where } \mathbf{G}^{U} \triangleq E(\mathbf{X}_k^{\mathscr{U}}\mathbf{U}_k^{\mathrm{T}}) = \mathbf{R}_0^{X^{\mathscr{U}}U}. \tag{13}$$

Algorithm A1 is the method in Section 2.1 applied to the *auto*-covariances $\mathbf{R}_i^{Y^{\mathscr{U}}Y^{\mathscr{U}}}$ in Eq. (12). The cross-covariances $\mathbf{R}_i^{Y^{\mathscr{U}}U}$ in Eq. (13) are to be handled in a combined manner; this is introduced in Algorithm A4 below.

2.2.2. Algorithm A2: eliminating the known input

For this algorithm, $(\mathbf{U}_k)$ does not need to be white. Thanks to assumptions in Eqs. (6) and (8), projecting Eq. (5) onto $\mathscr{U}^{\perp}$ amounts to eliminating the known input $\mathbf{U}$ (which does not need to be white). This projection writes:

$$\begin{cases} \mathbf{X}_k/\mathscr{U}^{\perp} = \mathbf{F}\mathbf{X}_{k-1}/\mathscr{U}^{\perp} + \mathbf{V}_k, \\ \mathbf{Y}_k/\mathscr{U}^{\perp} = \mathbf{H}\mathbf{X}_{k-1}/\mathscr{U}^{\perp} + \varepsilon_k. \end{cases} \tag{14}$$

Thus, setting for short $\mathbf{Z}^{\perp} = \mathbf{Z}/\mathscr{U}^{\perp}$, we get:

$$\begin{cases} \mathbf{X}_k^{\perp} = \mathbf{F}\mathbf{X}_{k-1}^{\perp} + \mathbf{V}_k, \\ \mathbf{Y}_k^{\perp} = \mathbf{H}\mathbf{X}_{k-1}^{\perp} + \varepsilon_k. \end{cases} \tag{15}$$

From Eq. (15), the following key decompositions for the covariance matrices holds:

$$\mathbf{R}_i^{Y^{\perp}Y^{\perp}} = \mathbf{H}\mathbf{F}^{i-1}\mathbf{G}^{Y^{\perp}}, \quad \text{where } \mathbf{G}^{Y^{\perp}} \triangleq E(\mathbf{X}_k^{\perp}\mathbf{Y}_k^{\perp\mathrm{T}}). \tag{16}$$

Since there are no known inputs to the system in Eq. (15), the method in Section 2.1 can be applied to the *auto-covariances* in Eq. (16). This is referred to as Algorithm A2.

2.2.3. Algorithm A3: using jointly both projections of Eq. (5) onto $\mathscr{U}$ and $\mathscr{U}^{\perp}$—Variant 1

For this algorithm, $(\mathbf{U}_k)$ is assumed white. This approach consists in combining the projections of the output $\mathbf{Y}_k$ onto both $\mathscr{U}$ and $\mathscr{U}^{\perp}$. Using $\overline{\mathbf{X}}_k \triangleq (\mathbf{X}_k^{\mathscr{U}}\ \ \mathbf{X}_k^{\perp})$ and $\overline{\mathbf{Y}}_k \triangleq (\mathbf{Y}_k^{\mathscr{U}}\ \ \mathbf{Y}_k^{\perp})$, the two systems in Eqs. (11) and (15) can be compacted into:

$$\begin{cases} \overline{\mathbf{X}}_k = \mathbf{F}\ \overline{\mathbf{X}}_{k-1} + (\mathbf{D}\mathbf{U}_k\ \ \mathbf{V}_k), \\ \overline{\mathbf{Y}}_k = \mathbf{H}\ \overline{\mathbf{X}}_{k-1} + (\mathbf{0}\ \ \varepsilon_k). \end{cases} \tag{17}$$

Consider the covariances:

$$\overline{\mathbf{R}}_i^Y \triangleq E[\mathbf{Y}_{k+i}(\mathbf{Y}_k^{\mathscr{U}\mathrm{T}} \;\; \mathbf{Y}_k^{\perp\mathrm{T}})]. \tag{18}$$

Note that:

$$E[\mathbf{Y}_{k+i} \;\; \mathbf{Y}_k^{\mathscr{U}\mathrm{T}}] = E[\mathbf{Y}_{k+i}^{\mathscr{U}} \;\; \mathbf{Y}_k^{\mathscr{U}\mathrm{T}}] = \mathbf{R}_i^{Y^{\mathscr{U}}Y^{\mathscr{U}}}, \tag{19}$$

$$E(\mathbf{Y}_{k+i} \;\; \mathbf{Y}_k^{\perp\mathrm{T}}) = E(\mathbf{Y}_{k+i}^{\perp} \;\; \mathbf{Y}_k^{\perp\mathrm{T}}) = \mathbf{R}_i^{Y^{\perp}Y^{\perp}}. \tag{20}$$

Thanks to Eqs. (19) and (20) and to Eqs. (12) and (16), we have:

$$\overline{\mathbf{R}}_i^Y = [\mathbf{R}_i^{Y^{\mathscr{U}}Y^{\mathscr{U}}} \;\; \mathbf{R}_i^{Y^{\perp}Y^{\perp}}] = \mathbf{H}\mathbf{F}^{i-1}[\mathbf{G}^Y \;\; \mathbf{G}^{Y^{\perp}}]. \tag{21}$$

Method in Section 2.1 applied to the *combined auto-covariances* in Eq. (21) is now called Algorithm A3.

2.2.4. Algorithm A4: using jointly both projections of Eq. (5) onto $\mathscr{U}$ and $\mathscr{U}^{\perp}$—Variant 2

For this algorithm, $(\mathbf{U}_k)$ is assumed white. Consider again the system in Eq. (17) with $(\mathbf{U})$ white and, now, the covariances:

$$\overline{\mathbf{R}}_i^U \triangleq E\left[\mathbf{Y}_{k+i}\left(\mathbf{U}_k^{\mathrm{T}} \;\; \mathbf{Y}_k^{\perp\mathrm{T}}\right)\right]. \tag{22}$$

Note that:

$$E[\mathbf{Y}_{k+i} \;\; \mathbf{U}_k^{\mathrm{T}}] = E[\mathbf{Y}_{k+i}^{\mathscr{U}} \;\; \mathbf{U}_k^{\mathrm{T}}] = \mathbf{R}_i^{Y^{\mathscr{U}}U}. \tag{23}$$

Thanks to Eqs. (23) and (20) and to Eqs. (13) and (16), we have:

$$\overline{\mathbf{R}}_i^U = [\mathbf{R}_i^{Y^{\mathscr{U}}U} \;\; \mathbf{R}_i^{Y^{\perp}Y^{\perp}}] = \mathbf{H}\mathbf{F}^{i-1}[\mathbf{G}^U \;\; \mathbf{G}^{Y^{\perp}}]. \tag{24}$$

Method in Section 2.1 applied to the *combined cross and auto-covariances* in Eq. (24) is called Algorithm A4.

2.2.5. Algorithm A5: ignoring the known input

For this algorithm, $(\mathbf{U}_k)$ is assumed white. One obvious way to ignore the presence of the known input $\mathbf{U}_k$ consists in performing output-only identification (namely regarding $\mathbf{D}\mathbf{U}_k + \mathbf{V}_k$ as a single unknown white noise). This way is a priori a loss of information, which is confirmed a posteriori when comparing input/output and output-only identification methods (Section 5). Recall that the output-only covariance-driven subspace identification of the eigenstructure is based on the method in Section 2.1 applied to the measured output covariances $\mathbf{R}_i \triangleq E(\mathbf{Y}_k \;\; \mathbf{Y}_{k-i}^{\mathrm{T}}) = \mathbf{R}_i^{YY}$, which we refer to as Algorithm A5.

2.2.6. Discussion

Subspace methods as described here share a lot of similarities with those described in Ref. [12]. Subspace methods in their more general form fit into two different categories. Either they try to recover the state matrices $(\mathbf{H}, \mathbf{F})$ from the observability matrix, or they try to recover these matrices from a state estimate. Our approach obviously fits into the first category, since we are using the left singular vectors of a weighted Hankel matrix. Different choices for the weights [21] can lead to different methods. Thus, the methods described here can be compared with existing methods like IV-4SID, basic-4SID, and MOESP [22,18] which is indeed very similar to Algorithm 4 above. Also, Algorithm 2 is of the same spirit as the projection algorithm for linear deterministic systems proposed in Ref. [12, Chapter 2]. Since we use different weights and different data stacking operations, we get different factorizations of the Hankel matrix. Thus, although in principle all these methods lead to the same left factor, they may have different numerical behaviors.

3. Polyreference LSCF for eigenstructure identification

The recent polyreference LSCF method [13–15] is a frequency domain method related in part to the basic PEM, when both inputs and outputs are available; see Ref. [23, Chapter 7] for single input single output

(SISO) systems, and Ref. [24, Appendix 4A, Chapter 7.3] for MIMO systems. By frequency domain method, we mean that measurements are directly collected in the Fourier domain, and are processed in the Fourier domain as well. This method is not new in its principle, but we feel it useful to review it and re-cast it in the classical system identification framework. Only an outline of the method is provided here. The reader is referred to Ref. [25] for the underlying system theoretic concepts, and to Refs. [13–15] for implementation details.

3.1. The input/output polyreference LSCF method

Throughout this section, we assume a N-size input/output time domain data sample $(\mathbf{Y}_k, \mathbf{U}_k)_k$. The DFT associated with a N-size vector data sample $(\mathbf{Z}_k)_k$ is generically denoted by: $\phi_N^Z(\omega) \triangleq 1/\sqrt{N}\sum_{k=1}^N \mathbf{Z}_k e^{-j\omega k}$, where $\omega = \omega_\ell \triangleq 2\pi\ell/N$, for $\ell = 1, \ldots, N$. We write ϕ^Z instead of ϕ_N^Z when the sample size N is understood. Let $\mathbf{S}(\omega)$ be the discrete Fourier domain matrix such that: $\phi^Y(\omega) = \mathbf{S}(\omega)\phi^U(\omega)$. Matrix $\mathbf{S}$ is called the FRF matrix. Its dimension is $r \times s$, r being the number of outputs and s being the number of inputs. The sequence $\mathbf{S}(\omega_\ell), \ell = 1, \ldots, N$, can be estimated from measurements in a non-parametric way (see Section 4.2). The polyreference LSCF method has two variants which are summarized now.

3.1.1. Left matrix-fraction description (LMFD)

In this variant, the system model is assumed under the form

$$\mathbf{A}(e^{-j\omega_\ell})\mathbf{S}(\omega_\ell) - \mathbf{B}(e^{-j\omega_\ell}) = \mathbf{V}(\omega_\ell) \quad \text{for } \ell = 0, \ldots, N, \tag{25}$$

where $\mathbf{A}(z) = \mathbf{A}_0 + \mathbf{A}_1 z + \cdots + \mathbf{A}_p z^p$ and $\mathbf{B}(z) = \mathbf{B}_0 + \mathbf{B}_1 z + \cdots + \mathbf{B}_q z^q$ are matrix polynomials, with size $r \times r$ and $r \times s$, respectively, and $\mathbf{V}(\omega_\ell)$, $\ell = 0, \ldots, N$ is a white noise matrix of suitable dimensions over the discrete unit circle. This model amounts to approximating the FRF matrix $\mathbf{S}$ by the LMFD form $\mathbf{A}^{-1}\mathbf{B}$. The eigenstructure of the system in Eq. (5)—modes and mode-shapes defined in Eq. (35)—is then recovered as the pairs (μ, ψ_μ) solutions of the eigenvalue problem:

$$\mathbf{A}(\mu)\psi_\mu = 0. \tag{26}$$

3.1.2. Right matrix-fraction description (RMFD)

In this variant, the system model is assumed under the form

$$\mathbf{S}(\omega_\ell)\mathbf{A}(e^{-j\omega_\ell}) - \mathbf{B}(e^{-j\omega_\ell}) = \mathbf{V}(\omega_\ell) \quad \text{for } \ell = 0, \ldots, N. \tag{27}$$

In this case, $\mathbf{A}$ and $\mathbf{B}$ are matrix polynomials, with size $s \times s$ and $r \times s$, respectively. This model amounts to approximating the FRF matrix $\mathbf{S}$ by the RMFD form $\mathbf{B}\mathbf{A}^{-1}$. The poles μ of system (5) are solutions of the following eigenvalue problem:

$$\mathbf{A}(\mu)\varphi_\mu = 0. \tag{28}$$

Note that the so-called *modal participation vector* φ_μ associated with μ in Eq. (28) is different from the mode-shape ψ_μ in Eq. (26). But the ψ_μ's can be easily recovered as follows. A LS approximation of $\mathbf{S}(\omega)$ by a partial fraction expansion having the μ's as its poles writes

$$\mathbf{S}(\omega) \approx \sum_{i=1}^{n/2}\left(\frac{\mathbf{T}_i}{j\omega - \mu_i} + \frac{\mathbf{T}_i^\star}{j\omega - \mu_i^*}\right), \tag{29}$$

where n is the system order (state dimension) and the superscript * denotes complex conjugate. Then, if there are no multiple poles, the residue matrices $\mathbf{T}_i$ have rank one. From Eq. (29), we get that $\mathbf{T}_i = \psi_{\mu_i}\varphi_{\mu_i}^T$, which yields the mode-shape ψ_{μ_i} [13].

Note that it is possible to include in Eq. (29) so-called residual terms, that take into account the effect of modes outside the frequency band that is being analyzed. This is rather classical, see for instance Ref. [4].

3.1.3. Discussion

- The two models in Eqs. (25) and (27) are linear in the parameters, with additive noise. Thus they can be identified via classical linear LS estimates; we refer the reader to Refs. [13–15] for implementation details. As it is well known [26,25], the MFD form (both left and right) suffers from non-identifiability problems, since, e.g., $\mathbf{A}^{-1}\mathbf{B}$ is invariant by pre-multiplication of both $\mathbf{A}$ and $\mathbf{B}$ by the same arbitrary invertible matrix. But this is of no harm in our case, since the eigenvalue problem in Eq. (26) is also invariant under the same pre-multiplication. Thus we only need to make sure that we find a maximal row rank MFD representation; the uniqueness of $\mathbf{A}$, however, is not our concern.
- If we ignore for a while the noise term in Eq. (25) for LMFD, then we can post-multiply this equation by $\mathbf{U}(\omega_\ell)$, and this yields the data based system model $\mathbf{AY}-\mathbf{BU}=0$. Reintroducing noise uncertainties gives raise to the popular linear LS PEM associated with the system model $\mathbf{AY}-\mathbf{BU}=\varepsilon$, that can be handled in both frequency or time domains [24]. However, this reasoning does not work for the RMFD variant, and we do not know how to relate this method to classical ones from the system identification literature in an easy way.
- Reasons for considering both variants are more practical than theoretical. Assume that there are many more inputs than outputs, i.e., $r \ll s$. Then, the order of matrix polynomial $\mathbf{A}$ is much larger in the usual LMFD representation $\mathbf{S}=\mathbf{A}^{-1}\mathbf{B}$ than in the RMFD representation $\mathbf{S}=\bar{\mathbf{B}}\bar{\mathbf{A}}^{-1}$. This favors choosing the LMFD representation, for the following reason: if we want to explore the LS solutions by assuming different model orders, increasing by one the order of polynomial $\mathbf{A}$ will increase the assumed model order (state dimension) by a smaller amount (see the discussion in Section 4.3 on the use of stabilization diagrams). Or course, the same arguments favor the RMFD representation $\mathbf{S}=\bar{\mathbf{B}}\bar{\mathbf{A}}^{-1}$ in the opposite case, where many more outputs are available than inputs. For modal analysis with *controlled* excitation, the second situation is the generic one, and therefore the non-classical RMFD representation is preferred.

For related discussions and additional information on this method, see Refs. [13,15].

3.2. The output-only polyreference LSCF method

Here we assume the model in Eq. (5) with $\mathbf{D}=0$, that is no measured input is available and the unmeasured input is assumed to be white noise. Let $\mathbf{S}(\omega)$ be the discrete Fourier domain matrix whose (i,j) entry equals $\phi^{Y_i}(\omega)\cdot(\phi^{Y_j}(\omega))^\star$, namely the measured cross-spectrum between the ith and jth outputs. Again, $\mathbf{S}(\omega_\ell), \ell=1,\ldots,N$ can be estimated from measurements in a non-parametric way (see Section 4.2).

The output-only polyreference LSCF method relies on the following basic fact from stochastic realization theory for linear systems [27]. Let $\mathbf{R}_Y(z)$ be the spectrum of $\mathbf{Y}$, expand it in a Fourier series $\mathbf{R}_Y(z)=\sum_{i=-\infty}^{+\infty}\mathbf{R}_i^{YY}z^i$, and set:

$$\mathbf{R}_Y^+(z)\triangleq\mathbf{R}_0^{YY}/2+\sum_{i=1}^{+\infty}\mathbf{R}_i^{YY}z^i,\quad \mathbf{R}_Y^-(z)\triangleq\mathbf{R}_0^{YY}/2+\sum_{i=-\infty}^{-1}\mathbf{R}_i^{YY}z^i.$$

The additive decomposition $\mathbf{R}_Y=\mathbf{R}_Y^+ + \mathbf{R}_Y^-$ holds, and $\mathbf{R}_Y^+$ is called the positive half-spectrum of $\mathbf{Y}$ and writes: $\mathbf{R}_Y^+(z)=\mathbf{H}(\mathbf{I}-z^{-1}\mathbf{F})^{-1}\mathbf{G}+\mathbf{J}$ with $\mathbf{J}=\mathbf{R}_0^{YY}/2$ and $\mathbf{G}=E(\mathbf{X}_k\mathbf{Y}_k^{\mathrm{T}})=\mathbf{R}_0^{XY}$. Then, approximating $\mathbf{R}_Y^+$ with a LMFD or RMFD representation as in Section 3.1 yields (estimates of) the poles of the system in Eq. (5). Finally, the corresponding mode-shapes are estimated using again partial fraction expansion of Eq. (29).

4. Implementation issues and testing requirements

First some implementation issues for the algorithms of Sections 2 and 3 are outlined. Second, constraints and requirements of the industrial testing practice, which should be kept in mind for the assessment of the practical applicability of the proposed methods, are discussed.

4.1. Implementation issues—subspace algorithms

4.1.1. Truncation

Of course, the doubly infinite linear space $\mathscr{U} = \text{Span}\{\mathbf{U}_j : -\infty < j < +\infty\}$ is not practical. However, if the input excitation has no pure frequency (multi-sine)[3] and if matrix $\mathbf{F}$ is stable (no root on the unit circle), then $(\mathbf{X}_k, \mathbf{Y}_k)$ is nearly independent of $\mathbf{U}_{k\pm m}$ for m large enough. Therefore $\mathscr{U}$ can be truncated and, in Eqs. (10), (14) and (17), it can be replaced by: $\mathscr{U}_k^{\mathrm{T}} = [\mathbf{U}_{k-m}^{\mathrm{T}} \ \ldots \ \mathbf{U}_k^{\mathrm{T}} \ \ldots \ \mathbf{U}_{k+m}^{\mathrm{T}}]$, which spans the truncated space $\text{Span}\{\mathbf{U}_j : k-m \leqslant j \leqslant k+m\}$. Then, the following explicit formulas can be used:

$$\mathbf{Y}_k^{\mathscr{U}} \approx \mathbf{Y}_k/\mathscr{U}_k \quad \text{and} \quad \mathbf{Y}_k^{\perp} \approx \mathbf{Y}_k - \mathbf{Y}_k/\mathscr{U}_k,$$
$$\text{where } \mathbf{Y}_k/\mathscr{U}_k = E(\mathbf{Y}_k\mathscr{U}_k^{\mathrm{T}})[E(\mathscr{U}_k\mathscr{U}_k^{\mathrm{T}})]^{\dagger}\mathscr{U}_k \tag{30}$$

and superscript † denotes the Moore–Penrose pseudo-inverse. The effect of these approximations on asymptotic properties can be analyzed with arguments similar to those in Refs. [19,20]; this will be reported elsewhere. The choice of integer parameters in subspace methods is analyzed in Ref. [28].

4.1.2. Empirical estimates

In Section 2 and Eq. (30), everything is based on true covariance matrices and on projections which again involve true covariances. The implementation consists in approximating the true covariances by their corresponding empirical forms. Generically, for a given N-size sample, referring to Eq. (9), $\mathbf{R}_i^{WZ}$ is replaced by $\widehat{\mathbf{R}}_i^{WZ} \triangleq 1/(N-i)\sum_{j=1}^{N-i}\mathbf{W}_{j+i}\,\mathbf{Z}_j^{\mathrm{T}}$. Similarly, for any projection, $\mathbf{Z}/\mathscr{U}$ is replaced by its empirical counterpart $\widehat{\mathbf{Z}}/\mathscr{U}$, which, by definition, is obtained using empirical covariance estimates.

Moreover, the argument in Section 2.1 needs to be slightly adjusted to accommodate the following two practical facts, namely: (i) because of the empirical covariance estimates, the factorization in Eq. (2) is only approximate, and (ii) only a finite amount of $\mathbf{R}_i$'s are available. Hence the Hankel matrix in Eq. (3) is truncated to p block-rows and q block-columns. Therefore, the factorization of Hankel matrix $\mathscr{H}_{p,q}(\mathbf{R})$ is only approximate. This means that

$$\mathscr{H}_{p,q}(\mathbf{R}) = \Gamma_p(\mathbf{H},\mathbf{F})\ \Xi_q(\mathbf{F},\mathbf{G}) + \ \text{residual}, \tag{31}$$

where Γ_p and Ξ_q are the truncated observability and controllability matrices, respectively. A standard way to obtain such a factorization consists in performing the singular value decomposition (SVD) of an empirical Hankel matrix $\widehat{\mathscr{H}} \triangleq \text{Hank}\left(\widehat{\mathbf{R}}_i^{WZ}\right)$, and its truncation at the desired model order. This yields, in the left factor, an estimate $\widehat{\Gamma}$ for the observability matrix Γ:

$$\widehat{\mathscr{H}} \approx \mathbf{U}\Delta\mathbf{V}^{\mathrm{T}} = (\mathbf{U}_1 \ \ \mathbf{U}_0)\begin{pmatrix}\Delta_1 & \mathbf{0}\\ \mathbf{0} & \Delta_0\end{pmatrix}\begin{pmatrix}\mathbf{V}_1^{\mathrm{T}}\\ \mathbf{V}_0^{\mathrm{T}}\end{pmatrix}, \tag{32}$$

$$\widehat{\Gamma} = \mathbf{U}_1\Delta_1^{1/2}, \quad \widehat{\Xi} = \Delta_1^{1/2}\mathbf{V}_1^{\mathrm{T}}. \tag{33}$$

An estimate of $\mathbf{H}$ is then found in the first block-row of $\widehat{\Gamma}$, and an estimate of $\mathbf{F}$ is obtained solving Eq. (4) in the LS sense, from which the estimated eigenstructure $(\widehat{\lambda}, \widehat{\Phi}_\lambda)$ can be deduced, as in Eq. (38). In the output-only case, this is known under the name of balanced realization (BR) algorithm [29]. It easily extends to the input/output one [30]. Our experience is that selecting $q = p+1$ in Eq. (31) is relevant [9]. Choosing $p \gg q$ yield a better LS estimate for $\mathbf{F}$. When p increases, the modal estimates should stabilize after a reasonable value. Plotting the estimates versus p provides an information on the minimal choice for p. Increasing q is not useful unless one wants to obtain very high order stabilization diagrams. Choosing $q \gg p$ is not useful, since the observalibity matrix is derived from the left factor of the SVD of $\widehat{\mathscr{H}}$.

[3] How to handle the presence of sinusoidal components for the input excitation ($\mathbf{V}_k$) is described in Refs. [17,9].

4.1.3. Weighting matrices

If we compute and truncate the SVD of a *weighted* empirical Hankel matrix $\widehat{\mathscr{H}}_W \triangleq \mathbf{W}_1 \widehat{\mathscr{H}} \mathbf{W}_2^{\mathrm{T}}$, with $\mathbf{W}_1$ and $\mathbf{W}_2$ two known invertible matrices, then the factors in Eq. (33) write: $\widehat{\Gamma} = \mathbf{W}_1^{-1} \mathbf{U}_W \Delta_W^{1/2}$ and $\widehat{\Xi} = \Delta_W^{1/2} \mathbf{V}_W^{\mathrm{T}} (\mathbf{W}_2^{\mathrm{T}})^{-1}$. A classical approach [31–33,21] is to normalize the data such that every singular value lies between 0 and 1, and thus represents the cosine of the angle between the subspaces of the future and the past data. This normalization helps avoiding numerical problems by balancing the effects of the main modes and the less energetic ones. In the output-only case, a usual way to proceed is to choose $\mathbf{W}_1$ and $\mathbf{W}_2$ as the inverses of the empirical covariances of the future and past output measurements. Then, the weighted empirical Hankel matrix $\widehat{\mathscr{H}}_W$ has norm 1. This approach is known as the canonical variate analysis (CVA) and is particularly useful when the order of the process $(\mathbf{X}_k)$ is unknown. Adapting this idea to the input/output method in Section 2.2 is easy.

4.2. Implementation issues—polyreference LSCF algorithms

The input/output polyreference LSCF algorithm of Section 3.1 uses non-parametric transfer function estimates as primary data, whereas its output-only counterpart in Section 3.2 requires empirical estimates of output spectra or output half-spectra. Extensive discussions on how to obtain these empirical estimates are available in the literature [34–36]. For instance, a popular transfer function estimate is the so-called "H1" estimate. It assumes noise-free input measurements and estimates the transfer function as the ratio of the cross-spectrum estimate between input and output and the power spectrum of the inputs. These spectra are obtained as non-parametric estimates such as the weighted averaged periodogram (also known as modified Welch's periodogram). A discussion on (half) spectrum estimates in a modal analysis context can be found in Ref. [37].

4.3. Implementation issues—stabilization diagrams

A typical problem in estimating a parametric model from data is the determination of the model order. For the present eigenstructure identification problem, the dimension n of the matrix $\mathbf{F}$ should be estimated. In the subspace algorithms of Section 2, this would amount to estimating p in Eq. (31) with $q = p + 1$. In the polyreference LSCF algorithms of Section 3, this would amount to estimating the denominator polynomial order p. Formal procedures estimate models of different orders and compare these models according to a quality criterion such as Akaike's Final Prediction Error or Rissanen's Minimum Description Length criterion [24]. However, practical experience with the application of system identification methods to structural dynamics data learned that it is a good idea to over-specify the model order; to compute the poles from the model; and to eliminate spurious numerical poles afterwards.

The so-called *stabilization diagram* [38,39] is a very practical tool to achieve this goal. To construct such a stabilization diagram, a repeated analysis of the same data set is performed, each time for a different model order. The pole values from each analysis are combined in a single diagram: the pole frequencies (y-axis) are plotted as functions of the model order (x-axis). The pole is indicated by a symbol in this diagram. Poles corresponding to the physical system appear at nearly identical frequency locations for every analysis, which is readily visible in the diagram. To point out that the frequency (resp. damping value and eigenvector) of a pole falls within certain bounds of the result obtained at a one-order lower model, specific symbols are used. The spurious numerical poles will not stabilize at all during this process and can be sorted out of the modal parameter data set more easily. Such stabilization diagrams are displayed in Section 5.

4.4. Industrial testing requirements

What is important, in view of the practical applicability of the various methods to full-scale problems, is the way they are able to cope with the constraints and requirements of the industrial testing practice. These include:

- The use of large numbers of response transducers: this may range from 8 to 16 responses in a flutter test, 128 or more sensors in a car road test, to a few hundreds in a laboratory vibration test, such as an aircraft

ground vibration test. This is useful for obtaining the mode-shapes, but may decrease the quality of the estimated modes.

- The subdivision of a test in "patches" or sensor groups, leading to non-simultaneously measured data. This may require to use multi-patch identification algorithms [20].
- Sensitivity to data preprocessing: re-sampling, re-synchronization, band-filtering, etc. The effect of filtering has been partially addressed in Ref. [40].
- The non-whiteness of the (unknown) excitation: e.g. there is no guarantee at all that the atmospheric turbulences can be considered as white noise. As explained above, only Algorithm A2 is robust to that.
- The non-stochastic nature of the excitation: sweeps, or impulses, through aircraft control surfaces, etc. Large size models should be handled using few sensors at a time.
- The superposition of large levels of harmonic components: e.g. helicopter rotor frequencies, car engine harmonics, turbine shaft or gear speeds, etc. These harmonics will most likely appear as system modes.
- Large data sample sizes, often contaminated with large measurement errors. The algorithms of Section 2 deal with sample errors.
- Large model sizes.
- Robustness to model inconsistencies: small variations in system behavior during the test or in-between subsequent "patches". This may also require online monitoring with a smaller sample size and sliding window.
- Robustness to non-stationary excitation. This has been investigated in Refs. [19,20] for output-only subspace methods, and will be addressed elsewhere for input/output ones.
- The ease of order selection, including the generation of non-physical poles. This has been investigated in Ref. [39].
- The computational efficiency, especially in view of large data sample sizes, large sensor counts, and large model orders. Large sample sizes increase the quality of subspace-based estimates, and decrease the gap between input–output and output-only algorithms. Large sensor counts and large model orders should not be considered together.
- The efficiency in estimating damping ratios. This issue is known to be more difficult than for frequencies [41].
- The capability to generate confidence intervals. Theoretical confidence intervals can be obtained from Refs. [22,42]. Empirical confidence intervals are obtained from stabilization diagrams. However, in a real experiment, the usefulness of confidence intervals may be limited, because the bias between the estimated and true values is difficult to estimate [46].

The answers to these questions are essential in the assessment of the practical applicability of the proposed methods. The next subsection contains a discussion of the problem of in-flight data analysis. More industrial examples can be found in the literature [9,6].

5. In-flight data example

We now report on identification results obtained with the algorithms of Sections 2 and 3 on real in-flight measurements provided by Avions Marcel Dassault within the Eurêka project FLITE. The data were over-sampled by a factor of 10; i.e. the sampling frequency being about 10 times the maximum frequency of interest. Successive data sets are available, and thus the evolution of the modal characteristics with the aircraft modifications, such as decreasing fuel mass in the tanks, and with different flight conditions (altitude and speed), can be tracked. The experiment involves one input (a pilot driven excitation) and 12 output sensors. Input and output time histories and spectra are displayed in Fig. 1.

The subspace-based modal analysis algorithms of Section 2 have been run using the Scilab Modal toolbox, which contains all these algorithms, among others [43,44]. The polyreference LSCF algorithms of Section 3, implemented under the name of PolyMAX, have been run using the LMS Test.Lab toolbox [45].

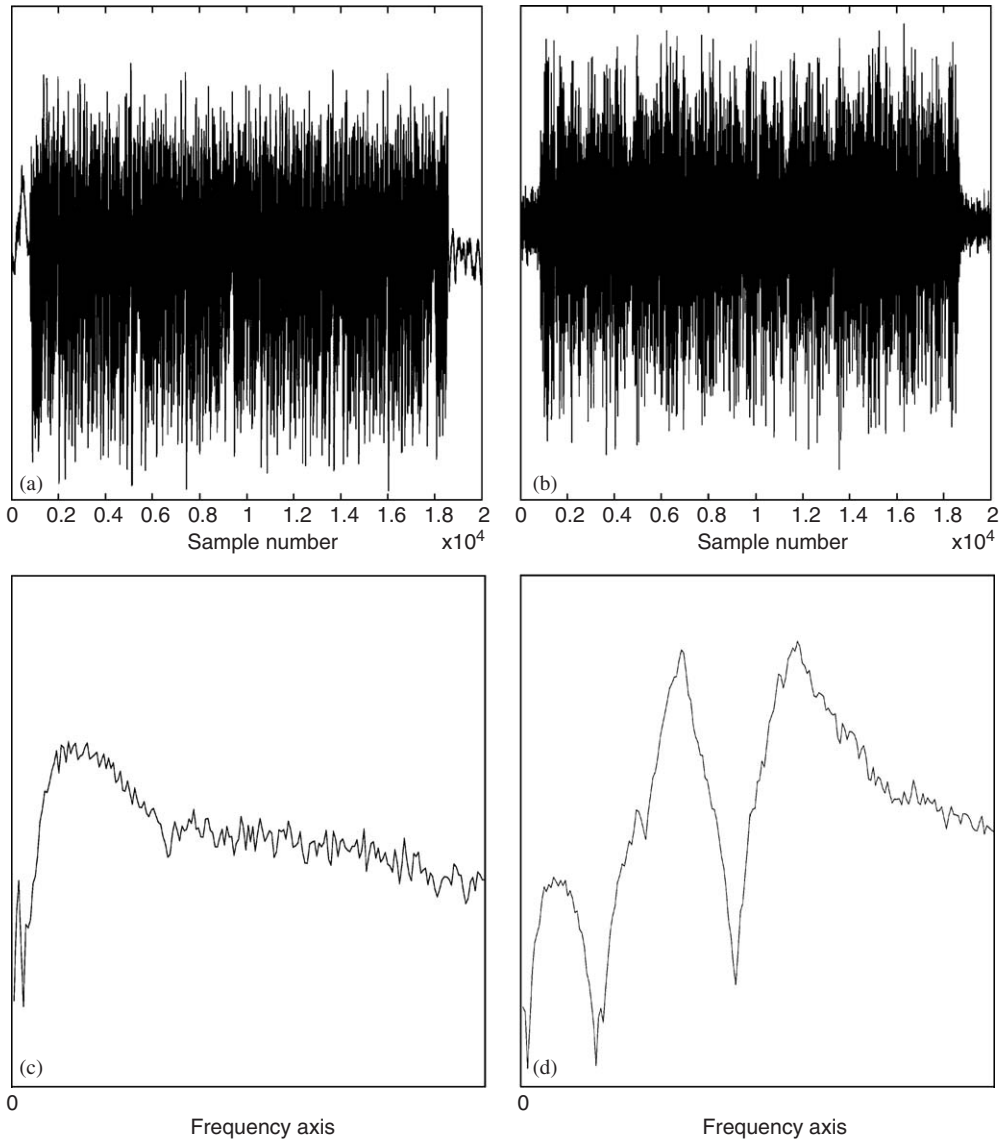

Fig. 1. Time histories and spectra: (a) 20 000 samples of input time history; (b) 20 000 samples of typical output time history; (c) lower part of input spectrum; (d) lower part of typical output spectrum.

5.1. Results with the subspace-based algorithms

We focus on the comparison of the output-only method with some of the input/output methods described in Section 2. All the methods have similar computational burden. They have been tested with different sample sizes: 5000, 10 000, 15 000 and 20 000 sample points.

It turns out that, *for the present example*, most input/output methods suffer from poor results, especially Algorithm A1. Because the observed artificial input is not white, it is intuitively natural that, *for the present example* again, the combined methods A3 and A4 do not perform as well as expected. These combined methods should be used preferably in experimental situations where the controlled input has better excitation properties. In the present example, the degree of correlation between the measured input and output signals is low, and some sensors are not well positioned for some modes. That is why we now focus on the merits of the output-only method (Algorithm A5) and the best input/output method (Algorithm A2).

In Figs. 2–7, the frequencies are displayed based on a classical stabilization diagram procedure and the alignments of the damping coefficients and of the modal assurance criterion (MAC) values are shown. The MAC is defined as the squared correlation coefficient between two modal vectors:

$$\mathrm{MAC}_{ij} \triangleq \frac{\|\psi^{\star}_{\mu_i}\psi_{\mu_j}\|^2}{(\psi^{\star}_{\mu_i}\psi_{\mu_i})(\psi^{\star}_{\mu_j}\psi_{\mu_j})}.$$

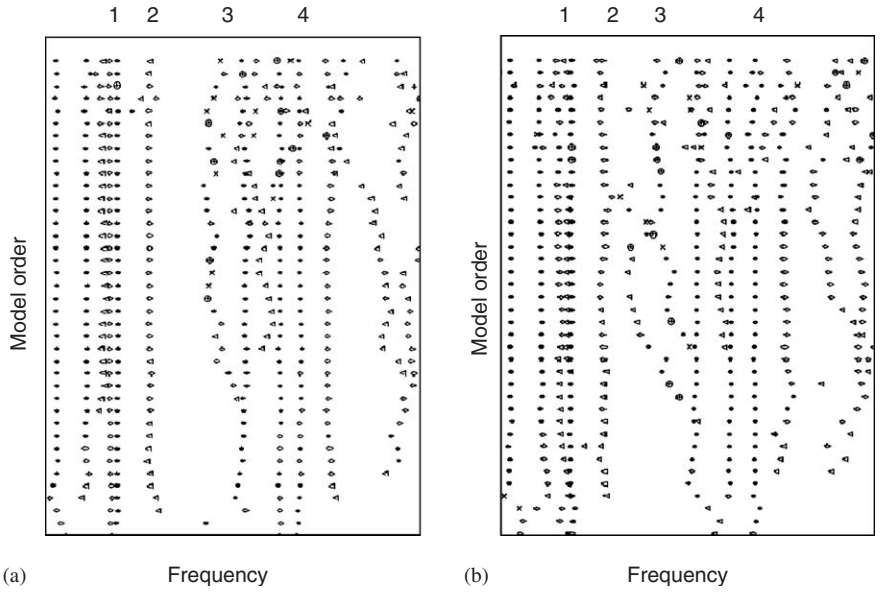

Fig. 2. Subspace algorithm—frequency stabilization diagram, 4 modes pointed out: (a) input/output; (b) output-only. X-axis: frequency, the range is about 25 Hz. Y-axis: number of block-rows in $\mathscr{H}$, the range is about 40. The key for damping coefficient d is: $\triangledown : d > 6\%$, $\diamond : 4\% < d \leqslant 6\%$, $\blacklozenge : 2\% < d \leqslant 4\%$, $\oplus : 1\% < d \leqslant 2\%$, $\times : 0.1\% < d \leqslant 1\%$, $+ : d \leqslant 0.1\%$.

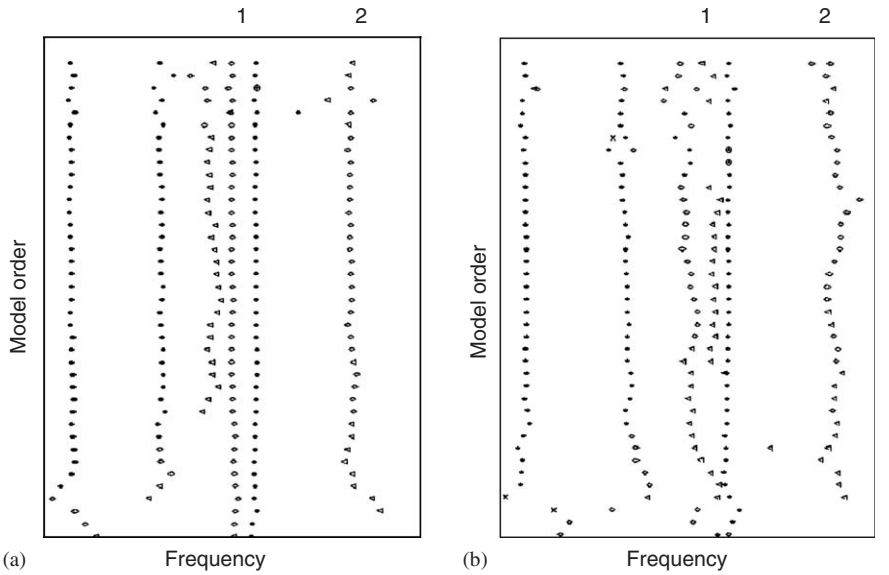

Fig. 3. Subspace algorithm—a closer look at 2 out of the 4 modes of Fig. 2: (a) input/output; (b) output-only. X-axis: frequency, the range is about 10 Hz. Y-axis as in Fig. 2.

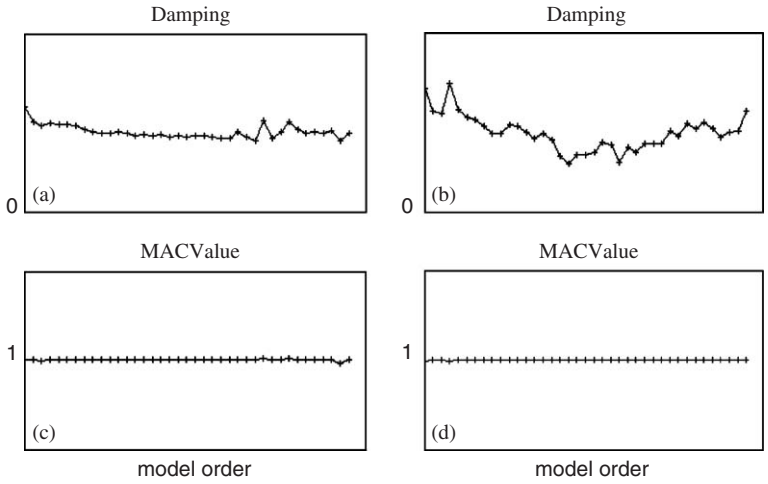

Fig. 4. Subspace algorithm—a closer look at mode 1 of Fig. 3: (a) damping coefficient with input/output; (b) damping coefficient with output-only; (c) MAC value with input/output; (d) MAC value with output-only. X-axis: as Y-axis in Fig. 2. Y-axis: the range is about 10% for (a) and (b), and 2 for (c) and (d).

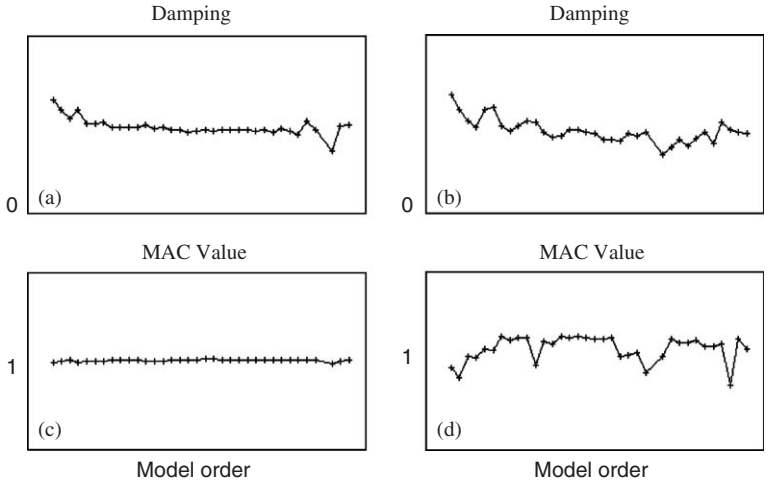

Fig. 5. Subspace algorithm—a closer look at mode 2 of Fig. 3: (a) damping coefficient with input/output; (b) damping coefficient with output-only; (c) MAC value with input/output; (d) MAC value with output-only. X and Y-axes: as in Fig. 4.

Note that there is no guarantee that the data delivered by the limited number of sensors enable the estimation of uncorrelated mode vectors and thus that all modes can be distinguished.

5.1.1. Input/output versus output-only

Both stabilization diagrams obtained with the same sample size (10 000) in the frequency range of interest are displayed in Fig. 2. It clearly appears that the input/output method yields more stable stabilization diagrams than the output-only approach. This appears still more clearly when zooming in the frequency band, as in Fig. 3. In addition to estimating the frequencies, we are also interested in good estimates of the damping coefficients and the mode-shapes. This can be evaluated by the quality of the damping alignment and of the MAC alignment. (Note that the latter is meaningful, because we are using enough sensors.) This is done for

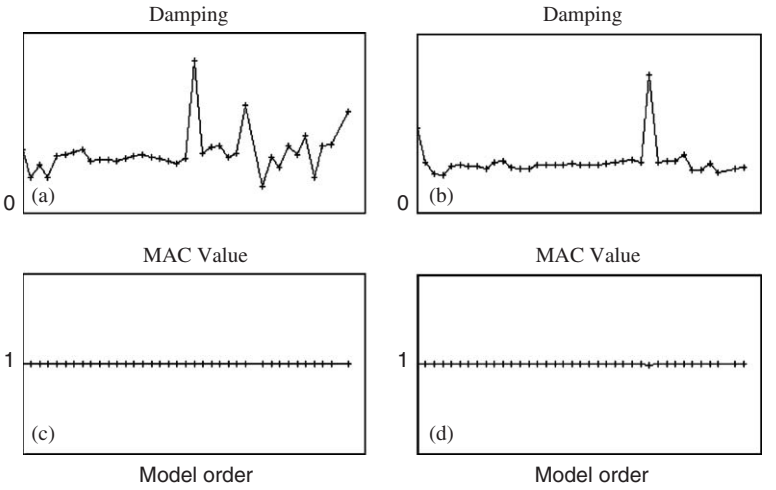

Fig. 6. Subspace algorithm—A5 (output-only), sample size effect for mode 4 of Fig. 2: (a) damping coefficient with 5000 samples; (b) damping coefficient with 10 000 samples; (c) MAC value with 5000 samples; (d) MAC value with 10 000 samples. X and Y-axes: as in Fig. 4.

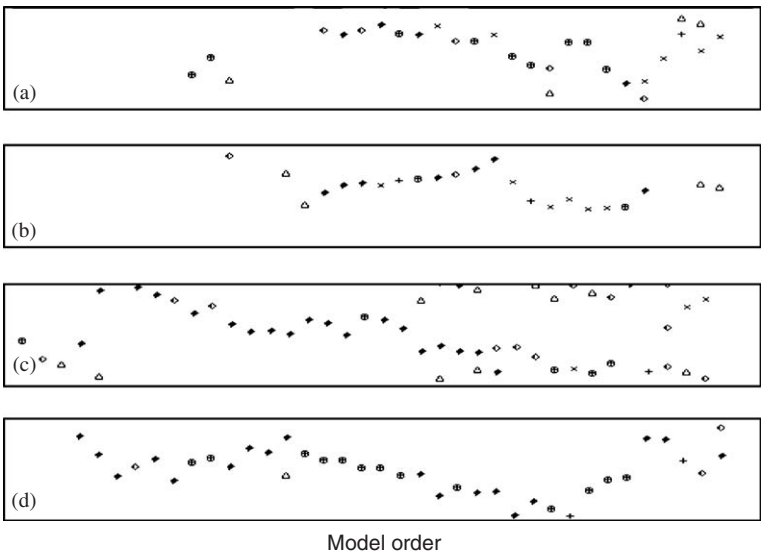

Fig. 7. Subspace algorithm—input effect on mode 3 of Fig. 2; (a) Algorithm A5: (b) Algorithm A2; (c) Algorithm A3; (d) Algorithm A4. X-axis and key: as in Fig. 2. Y-axis: the range is about 0.5 Hz for each plot.

two specific modes in Figs. 4 and 5. Comparing the quality of the stabilization diagrams of each method provides a good information on the superiority of the input/output approach.

5.1.2. *Sample size effect*

Both methods get better stabilization diagram as the size of the sample used for the identification increases. The input/output results are better than the output-only ones, but the difference in the performances of the input/output and output-only methods decreases when the sample size increases. An example of how the output-only estimates improves when using higher sample sizes is displayed in the damping and MAC

diagrams in Fig. 6. However, it appears that, when processing small records, the input/output method is better than the output-only one.

The subspace methods are only supposed to converge when the sample size goes to infinity and the variance for the output-only method will in general be higher than for the input/output one. However, results obtained from a *single* experiment should be distinguished from asymptotic properties provided by a statistical analysis. It may happen indeed that good estimates can be obtained with the output-only method, which performs sometimes better than its input/output counterpart.

5.1.3. Merits of using the input

In the results above, we have withdrawn all the input/output approaches, except for Algorithm A2, because they gave worse stabilization diagrams. Nonetheless, for some modes, it may happen that these methods yield better estimation results. An example of such a situation is displayed in Fig. 7, where it can be seen that, *for that particular mode*, the combined approaches Algorithms A3 and A4 give the best (albeit not really good) estimates. For all the other modes, the input/output approaches except for Algorithm A2 gave significantly worse results looking at all frequencies, damping coefficients and MAC's altogether.

This suggests that the input/output subspace Algorithms A1, A3 and A4 in Section 2 may have better performance in other applications, when the input signal has better properties, most likely in strictly controlled experiments as in laboratory setups. From a theoritical point of view, using input will always improve the methods, as long as the input signal is close to the assumptions. The subspace output-only Algorithm A5 has been proved to be robust to non-stationary excitation [19]. Consistency and asymptotic normality have been proved for a class of similar subspace methods in Ref. [42]. However, no theoritical consistency result is available when the identification algorithm handles a model structure (order) which is not the true one.

5.2. Results with the polyreference LSCF algorithms

Both the input/output and output-only versions of the polyreference LSCF method have been applied to data records of different lengths: 10 000, 15 000, 20 000 samples. When processing the time data into FRF's, the frequency resolution was kept constant (0.1 Hz). So the number of averages depend on the data length: respectively, 7, 11, 15 averages for 10 000, 15 000, 20 000 samples. A Hanning window was used and an overlap between the data segments of 50%.

In the output-only case, the cross spectra between the outputs and two selected reference outputs served as primary data. In the input/output case, the FRF's between the single input and all the outputs served as primary data. In order to obtain models with the same number of modes, the maximum denominator polynomial order in the input/output case was chosen to be twice the order in the case of the output-only data.

5.2.1. Input/output versus output-only

Although the stabilization quality is good in both cases of Fig. 8, it seems that more stable poles are found when including the input information. When looking at the frequency and damping evolution as a function of the model order as displayed in Figs. 9 and 10, a positive effect of using the input information is visible: the variation of the output-only poles is larger. From these pictures, it is also clear that the input/output and output-only pole estimates do not coincide. This is probably due to the (slight) coloring of the inputs. A coloring of the inputs may be the cause of the fact that poles estimated from the transfer function between input and output are not the same as the poles only identified from the outputs and assuming a white noise input.

5.2.2. Sample size effect

Changing the sample size is not changing the aspect of the stabilization diagrams dramatically (see Fig. 8). From Figs. 9 and 10, it can be concluded that the frequency and damping variations as a function of model order slightly decreases when more samples are used.

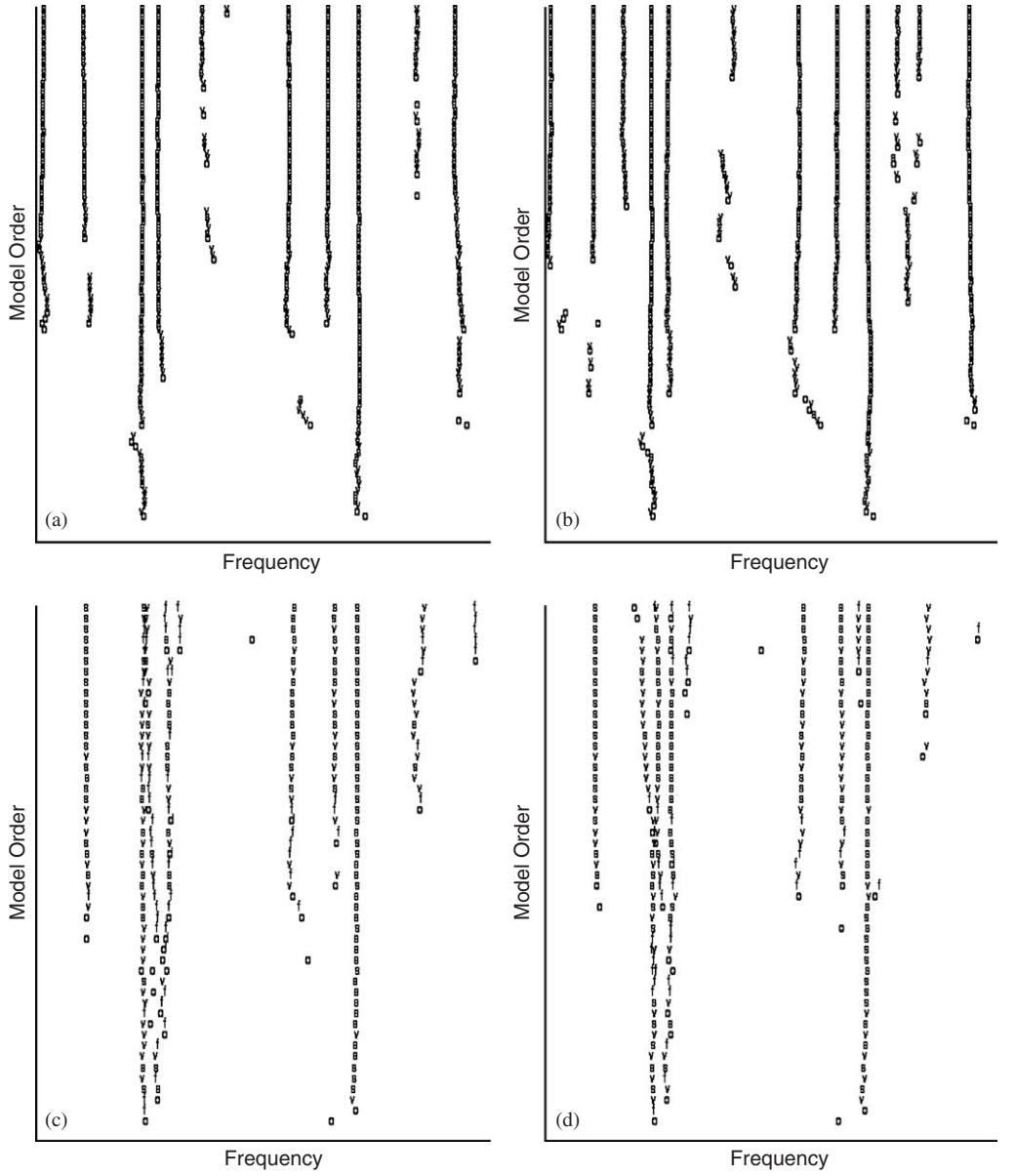

Fig. 8. LSCF algorithm—frequency stabilization diagrams, sample size effect: (a) input/output data, 10 000 samples; (b) input/output data, 20 000 samples; (c) output-only data, 10 000 samples; (d) output-only data, 20 000 samples. X-axis: the range is about 20 Hz. Y-axis: order of polynomial A.

6. Further comments and conclusions

We have discussed two classes of eigenstructure identification methods, the subspace and polyreference LSCF methods, each working with either input/output or output-only data.

We have presented the practical capabilities of both classes of methods for non-stationary aircraft structures. For the subspace-based algorithms, the experimental results show that the input/output method performs better than the output-only one on real data. For long samples, the loss in accuracy becomes negligible. For small sample sizes, the additional value of using inputs—when available—may be significant. For the polyreference LSCF methods, similar conclusions can be drawn.

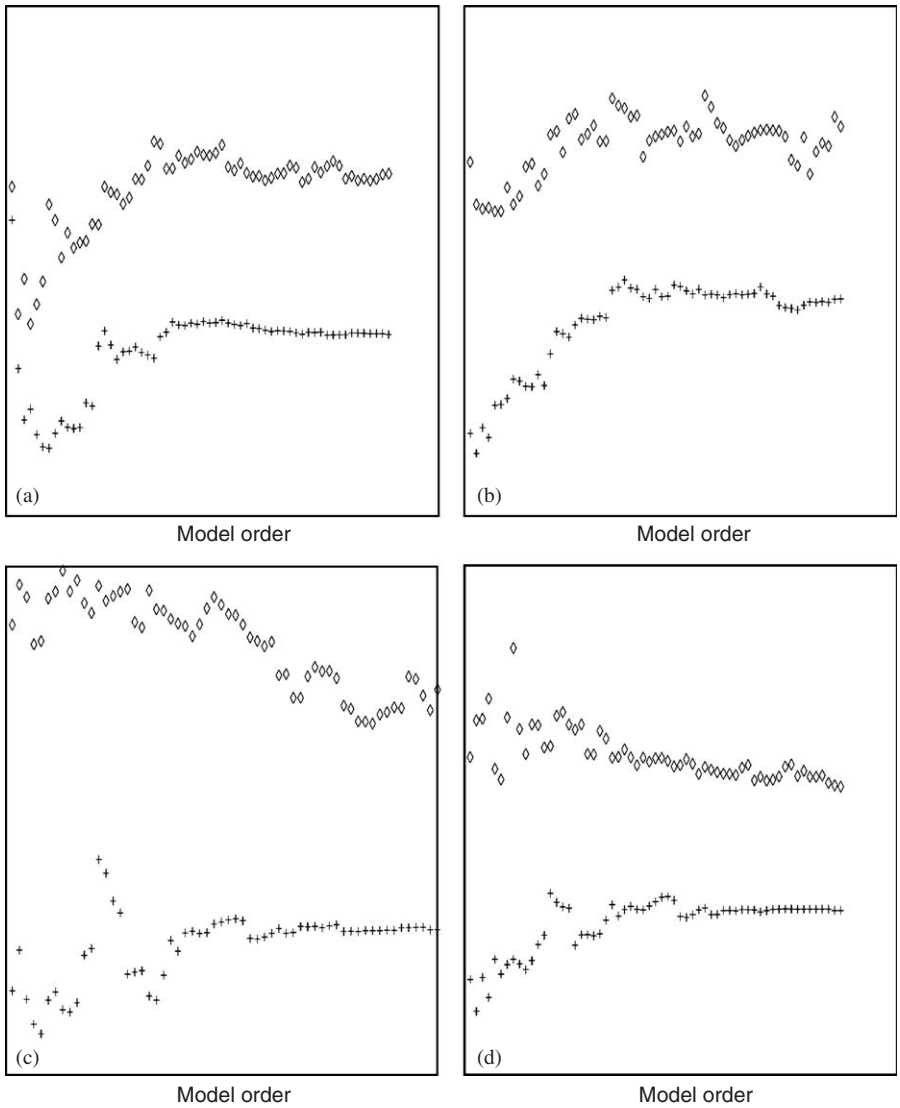

Fig. 9. LSCF algorithm—a closer look at the frequencies of two modes of Fig. 8, sample size effect: (a) first mode, 10 000 samples; (b) first mode, 20 000 samples; (c) second mode, 10 000 samples; (d) second mode, 20 000 samples. +: Input/output, ◇: output-only. X-axis: as Y-axis in Fig. 8. Y-axis: the range is about 1 Hz.

The lesson from this paper is that, when easily available, input sensor data should be used. Of course, when inputs are not measured, only the output-only methods can be used, and our study demonstrates that this a reasonable approach. In some cases, using input measurements or not may result from a trade-off between sensors cost and increased estimation accuracy.

As for the subspace-based methods in Section 2, Algorithm A2 is preferable when the input is available or the sample size is short; Algorithm A5 when the sample size increases or no input is available; the other algorithms should not be considered unless $\mathbf{U}$ is white.

Concerning the polyreference LSCF methods discussed in Section 3, experience has shown that the method that identifies a RMFD model yields very clear stabilization diagrams: in the most typical situation more outputs than inputs (or references) are available, so a RMFD stabilization diagram encompasses a large amount of polynomial orders (and thus lines in the diagram) for a certain number of poles; and it turns out that the identified poles remain very stable when increasing the polynomial order.

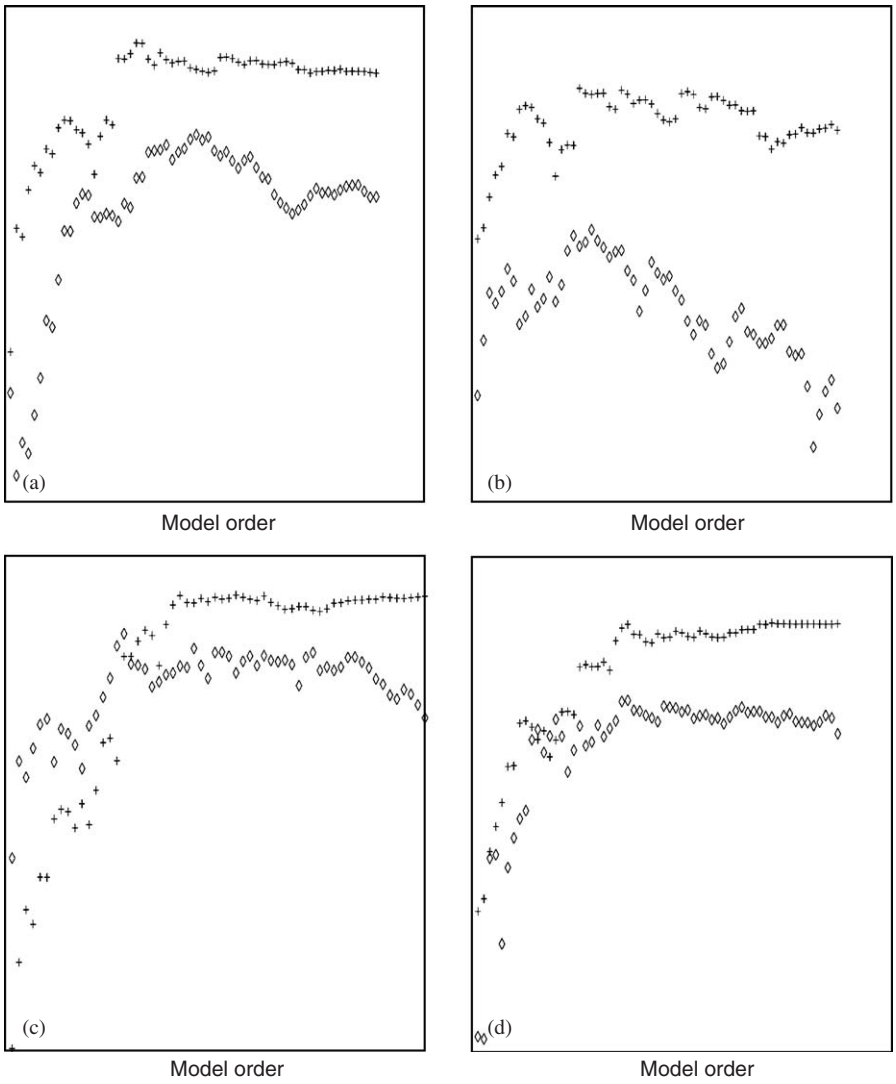

Fig. 10. LSCF algorithm—the damping coefficients for the two modes in Fig. 9: (a) first mode, 10 000 samples; (b) first mode, 20 000 samples; (c) second mode, 10 000 samples; (d) second mode, 20 000 samples. X-axis and key: as in Fig. 9. Y-axis: the range is about 2%.

Acknowledgments

The authors are indebted to the editor and the referees, whose careful reading and comments helped improving an earlier version of the paper. The contribution of Arnaud Guyader to an early version of the subspace-based input/output methods described in Section 2, of Yann Veillard to the development of the Scilab toolbox, and of Auguste Sam to the experimental results in Section 5, are acknowledged. This work has been carried out within and supported by the Eureka projects no. 1562 SINOPSYS (Model based Structural monitoring using in-operation system identification) coordinated by LMS, Leuven, Belgium, and no. 2419 FLITE (Flight Test Easy), coordinated by Sopemea, Velizy-Villacoublay, France.

Appendix. State-space model for structural analysis

The use of state-space representations for modal analysis is well known [4,5,8]. For the sake of completeness, we briefly recall the main equations and parameters. We assume that the behavior of the system

can be described by a stationary linear dynamical system, and that, in the frequency range of interest, the input forces can be modeled as a non-stationary white noise. Consequently, the relevant model is the matrix differential system:

$$\begin{cases} \mathbf{M}\ddot{\mathscr{Y}}(t) + \mathbf{C}\dot{\mathscr{Y}}(t) + \mathbf{K}\mathscr{Y}(t) = \mathbf{B}\Upsilon(t) + v(t), \\ \mathbf{Y}(t) = \mathbf{L}\mathscr{Y}(t) + \varepsilon(t), \end{cases} \tag{34}$$

where t denotes continuous time, $\mathbf{M}, \mathbf{C}, \mathbf{K}$ are the mass, damping and stiffness matrices respectively; (high dimensional) vector $\mathscr{Y}$ collects the displacements of the degrees of freedom of the structure; vector Υ contains the known input, assumed to be de-correlated from both v and ε (and thus not a feedback); the unknown external force v is modeled as a stationary white noise[4] with covariance matrix $\mathbf{Q}_v$; measurements are collected in the (often, low dimensional) vector $\mathbf{Y}$; matrix $\mathbf{L}$ states where the sensors are located and matrix $\mathbf{B}$ where the forces are applied; and ε is a white measurement noise, de-correlated from v (and Υ).

The *mode-frequencies* or eigenfrequencies denoted generically by μ, and the *mode-shapes* or eigenvectors denoted generically by ψ_μ, are solutions of

$$\det(\mathbf{M}\mu^2 + \mathbf{C}\mu + \mathbf{K}) = 0, \quad (\mathbf{M}\mu^2 + \mathbf{C}\mu + \mathbf{K})\Psi_\mu = 0, \quad \psi_\mu = \mathbf{L}\Psi_\mu. \tag{35}$$

Sampling the model in Eq. (34) at rate $1/\tau$ yields the discrete time model in state space form

$$\begin{cases} \mathbf{X}_k = \mathbf{F}\mathbf{X}_{k-1} + \mathbf{D}\mathbf{U}_k + \mathbf{V}_k, \\ \mathbf{Y}_k = \mathbf{H}\mathbf{X}_{k-1} + \varepsilon_k, \end{cases} \tag{36}$$

where the state, input and output are:

$$\mathbf{X}_k = \begin{bmatrix} \mathscr{Y}(k\tau) \\ \dot{\mathscr{Y}}(k\tau) \end{bmatrix}, \quad \mathbf{U}_k = \begin{bmatrix} \mathbf{0} \\ \Upsilon(k\tau) \end{bmatrix}, \quad \mathbf{Y}_k = \mathbf{Y}(k\tau), \tag{37}$$

the state transition, the state input gain and the observation matrices are:

$$\mathbf{F} = \mathrm{e}^{\mathscr{L}\tau} \text{ with } \mathscr{L} = \begin{bmatrix} \mathbf{0} & \mathbf{I} \\ -\mathbf{M}^{-1}\mathbf{K} & -\mathbf{M}^{-1}\mathbf{C} \end{bmatrix}, \quad \mathbf{D} = \begin{bmatrix} \mathbf{0} & \mathbf{0} \\ \mathbf{0} & \mathbf{B} \end{bmatrix}, \quad \mathbf{H} = [\mathbf{L} \ \ \mathbf{0}]$$

and where state noise $\mathbf{V}_k$ contains an *unknown*, Gaussian, zero-mean, white noise $\mathbf{V}_k$, with covariance matrix: $\mathbf{Q}_k \triangleq E(\mathbf{V}_k \ \ \mathbf{V}_k^{\mathrm{T}})$, where $E(.)$ denotes the expectation operator. Known input $\mathbf{U}$, state $\mathbf{X}$ and observed output $\mathbf{Y}$ have dimensions $s, n = 2m$ and r, respectively, with r (often much) smaller than n in practice. The assumptions on the known input $\mathbf{U}_k$ and the unknown noises $\mathbf{V}_k$ and ε_k are further discussed in Section 2.2.

The eigenstructure (λ, Φ_λ) of the state transition matrix $\mathbf{F}$ results from:

$$\det(\mathbf{F} - \lambda\mathbf{I}) = 0, \quad \mathbf{F}\Phi_\lambda = \lambda\Phi_\lambda \tag{38}$$

and the modal parameters defined in Eq. (35) are then deduced as: $\mathrm{e}^{\tau\mu} = \lambda$, $\psi_\mu = \varphi_\lambda \triangleq \mathbf{H}\Phi_\lambda$. The frequency and damping coefficient are recovered from a given eigenvalue λ through:

$$\text{Frequency} = \frac{a}{2\pi\tau}, \quad \text{Damping} = \frac{100|b|}{\sqrt{a^2 + b^2}}, \quad a = \left|\arctan\frac{\mathrm{Im}(\lambda)}{\mathrm{Re}(\lambda)}\right|, \quad b = \ln|\lambda|.$$

Eigenvectors are real if $\mathbf{C} = \alpha\mathbf{M} + \beta\mathbf{K}$, the simplest form of proportional damping. Because of the structure of the state in Eq. (37), the λ's and φ_λ's are pairwise complex conjugate. It is assumed that the system has no multiple eigenvalues. In addition, 0 is *not* an eigenvalue of state transition matrix $\mathbf{F}$. The collection of pairs $(\lambda, \varphi_\lambda)$ form a canonical parameterization[5] of the pole part of the system in Eq. (36), referred to as the system eigenstructure.

[4]The non-stationary case is addressed in Refs. [19,20].

[5]A parameterization invariant w.r.t. changes in the state basis.

References

[1] R. Jategaonkar, D. Fischenberg, W. von Gruenhagen, Aerodynamic modeling and system identification from flight data—recent applications at DLR, *AIAA Journal of Aircraft* 41 (2004) 681–691.

[2] C.R. Pickrel, P.J. White, Flight flutter testing of transport aircraft: in-flight modal analysis, *Proceedings of the 21st International Modal Analysis Conference*, Kissimmee, Florida, 2003, Paper No. 200.

[3] M.W. Kehoe, A historical overview of flight flutter testing, NASA Technical Memorandum 4720, 1995.

[4] D.J. Ewins, *Modal Testing: Theory, Practice and Applications*, second ed., Research Studies Press, Letchworth, Hertfordshire, UK, 2000.

[5] J.N. Juang, *Applied System Identification*, Prentice-Hall, Englewood Cliffs, NJ, 1994.

[6] B. Peeters, G. De Roeck, Stochastic system identification for operational modal analysis: a review, *ASME Journal of Dynamic Systems Measurement and Control* 123 (2001) 659–667.

[7] F. Deblauwe, R.J. Allemang, D. l. Brown, The polyreference time domain technique, *Proceedings of the Fifth International Modal Analysis Conference*, 1987, pp. 832–845.

[8] B. Peeters, G. De Roeck, Reference-based stochastic subspace identification for output-only modal analysis, *Mechanical Systems and Signal Processing* 13 (1999) 855–878.

[9] M. Basseville, A. Benveniste, M. Goursat, L. Hermans, L. Mevel, H. Van der Auweraer, Output-only subspace-based structural identification: from theory to industrial testing practice, *ASME Journal of Dynamic Systems Measurement and Control* 123 (2001) 668–676.

[10] B. Ottersten, M. Viberg, T. Kailath, Analysis of subspace fitting and ML techniques for parameter estimation, *IEEE Transactions on Signal Processing* 40 (1992) 590–599.

[11] M. Viberg, Subspace-based methods for the identification of linear time-invariant systems, *Automatica* 31 (1995) 1835–1853.

[12] P. Van Overschee, B. De Moor, *Subspace Identification for Linear Systems: Theory—Implementation—Applications*, Kluwer Academic Publishers, Dordrecht, NL, 1996.

[13] P. Guillaume, P. Verboven, S. Vanlanduit, H. Van der Auweraer, B. Peeters, A polyreference implementation of the least-squares complex frequency domain estimator, *Proceedings of the 21st International Modal Analysis Conference*, Kissimmee, FL, 2003, Paper No. 183.

[14] B. Peeters, P. Guillaume, H. Van der Auweraer, B. Cauberghe, P. Verboven, J. Leuridan, Automotive and aerospace applications of the PolyMAX modal parameter estimation method, *Proceedings of the 22nd International Modal Analysis Conference*, Dearborn, MI, 2004, Paper No. 199.

[15] B. Cauberghe, P. Guillaume, P. Verboven, E. Parloo, S. Vanlanduit, A polyreference implementation of the maximum likelihood complex frequency-domain estimator and some industrial applications, *Proceedings of the 22nd International Modal Analysis Conference*, Dearborn, MI, 2004, Paper No. 179.

[16] M. Basseville, M. Abdelghani, A. Benveniste, Subspace-based fault detection algorithms for vibration monitoring, *Automatica* 36 (2000) 101–109.

[17] M. Prevosto, M. Olagnon, A. Benveniste, M. Basseville, G. LeVey, State-space formulation, a solution to modal parameter estimation, *Journal Sound and Vibration* 148 (1991) 329–342.

[18] M. Abdelghani, C.T. Chou, M. Verhaegen, Using subspace methods in the identification and modal analysis of structures, *Proceedings of the 15th International Modal Analysis Conference*, Orlando, FL, 1997, pp. 1392–1398.

[19] A. Benveniste, J.-J. Fuchs, Single sample modal identification of a nonstationary stochastic process, *IEEE Transactions on Automatic Control* 30 (1985) 66–74.

[20] L. Mevel, A. Benveniste, M. Basseville, M. Goursat, Blind subspace-based eigenstructure identification under non-stationary excitation using moving sensors, *IEEE Transactions on Signal Processing* 50 (2002) 41–48.

[21] D. Bauer, L. Ljung, Some facts about the choice of the weighting matrices in Larimore type of subspace algorithms, *Automatica* 38 (2002) 763–773.

[22] D. Bauer, M. Jansson, Analysis of the asymptotic properties of the MOESP type of subspace algorithms, *Automatica* 36 (2000) 497–509.

[23] T. Soderström, P. Stoïca, *System Identification*, Prentice Hall International Series in Systems and Control Engineering, 1989.

[24] L. Ljung, *System Identification—Theory for the User*, second ed., PTR Prentice-Hall, Upper Saddle River, NJ, 1999.

[25] T. Kailath, *Linear Systems*, Prentice Hall, NJ, 1980.

[26] E.J. Hannan, M. Deistler, *The Statistical Theory of Linear Systems*, Wiley Series in Probability and Mathematical Statistics, 1988.

[27] P.E. Caines, *Linear Stochastic Systems*, Wiley Series in Probability and Mathematical Statistics, 1988.

[28] D. Bauer, Choosing integer parameters in subspace methods: a survey on asymptotic results, *Proceedings of the 13th IFAC/IFORS Symposium on Identification and System Parameter Estimation*, Rotterdam, NL, 2003, Paper No. ISC-77.

[29] H. Akaïke, Stochastic theory of minimal realization, *IEEE Transactions on Automatic Control* 19 (1974) 667–674.

[30] A. Guyader, L. Mevel, Covariance-driven subspace methods: input/output vs. output-only, *Proceedings of the 21st International Modal Analysis Conference*, Kissimmee, FL, 2003, Paper No. 136.

[31] H. Akaïke, Markovian representation of stochastic processes by canonical variables, *SIAM Journal of Control* 13 (1973) 162–173.

[32] K.S. Arun, S.Y. Kung, Generalized principal components analysis and its application in approximate stochastic realization, in: U.B. Desai (Ed.), *Modeling and Application of Stochastic Processes*, Kluwer Academic Publishers, Dordrecht, 1986, pp. 75–103.

[33] A. Lindquist, G. Picci, Canonical correlation analysis, approximate covariance extension, and identification of stationary time series, *Automatica* 32 (1996) 709–733.
[34] S.L. Marple, *Digital Spectral Analysis*, Prentice-Hall, New York, USA, 1987.
[35] P. Guillaume, R. Pintelon, J. Schoukens, Accurate estimation of multivariable frequency response functions, *Proceedings of the 13th IFAC Triennal World Conference*, San Francisco, CA, 1996, pp. 423–428.
[36] R. Pintelon, J. Schoukens, *System Identification: A Frequency Domain Approach*, IEEE Press, New York, USA, 2001.
[37] L. Hermans, H. Van der Auweraer, P. Guillaume, A frequency-domain maximum likelihood approach for the extraction of modal parameters from output-only data, *Proceedings of ISMA23, the International Conference on Noise and Vibration Engineering*, Leuven, Belgium, 1998, pp. 367–376.
[38] W. Heylen, S. Lammens, P. Sas, *Modal Analysis Theory and Testing*, Mechanical Engineering Department, Katholieke Universiteit Leuven, Leuven, Belgium, 1995.
[39] H. Van der Auweraer, B. Peeters, Discriminating physical poles from mathematical poles in high order systems: use and automation of the stabilization diagram, *Proceedings of the IEEE Instrumentation and Measurement Technology Conference*, Como, Italy, 2004.
[40] L. Mevel, A. Sam, M. Goursat, Blind modal identification for large aircrafts—The case of a high number of close poles, *Proceedings of the 22nd International Modal Analysis Conference*, Dearborn, MI, 2004, Paper No. 66.
[41] W. Gersch, On the achievable accuracy of structural parameter estimates, *Journal of Sound and Vibration* 34 (1974) 63–79.
[42] A. Chiuso, G. Picci, On the ill-conditioning of subspace identification with inputs; Numerical conditioning and asymptotic variance of subspace estimates, *Automatica* 40 (2004) 575–589.
[43] L. Mevel, M. Goursat, A. Benveniste, Using subspace on flight data, a practical example, *Proceedings of the 21st International Modal Analysis Conference*, Kissimmee, FL, 2003, Paper No. 138.
[44] L. Mevel, M. Goursat, M. Basseville, A. Benveniste, Subspace-based modal identification and monitoring of large structures, a Scilab toolbox, *Proceedings of the 13th IFAC/IFORS Symposium on Identification and System Parameter Estimation*, Rotterdam, NL, 2003, Paper No. ISC-53. (Downloadable from http://www.irisa.fr/sisthem/cosmad)
[45] LMS International, *LMS Test.Lab—Structural Testing Rev 4B*, Leuven, Belgium, 2004. (More information on http://www.lmsintl.com)
[46] M. Goursat, L. Mevel, Using subspace on a large aircraft dataset, a case study, *Proceedings of the 23rd International Modal Analysis Conference*, Orlando, FL, 2005, Paper No. 120.